ACS OMEGA

Open Access

http://pubs.acs.org/journal/acsodf

Article

Probing the Thermochemistry Properties and Rate Kinetics of Trimethyl Phosphate (TMP): An H-Atom Abstraction (HAA) Reactions Perspective

Frederick Nii Ofei Bruce and Yang Li*

Cite This: *ACS Omega* 2023, 8, 47134−47145

Read Online

ACCESS | Metrics & More | Article Recommendations | Supporting Information

ABSTRACT: Trimethyl Phosphate (TMP), an organophosphorus liquid compound, is valued for its versatile qualities and applications in various fields. In modern chemical research and industry, processes involving Trimethyl Phosphate are optimized for minimal negative environmental impact, and scientific advancement is driven by adherence to stringent regulations to provide sustainable solutions and resource preservation. Thermochemical insights enhance our understanding of monomer incorporation, initiation, and propagation energetics. This study comprehensively investigates the thermochemistry and rate kinetics that govern H-atom abstractions in TMP through advanced computational techniques. The theoretical framework encompasses methodologies for conducting conformer searches, exploring transition states, and performing energy calculations. This study calculates rate constants for eight H-atom abstraction reactions involving TMP with stable species, O_2 (oxygen), H (hydrogen), and radicals [$\dot{O}H$ (hydroxyl), $\dot{C}H_3$ (methyl), $CH_3\dot{O}$ (methoxy), $H\dot{O}_2$ (hydroperoxyl), $\dot{N}H_2$ (amino), and $\dot{C}N$ (cyano)], and further analogies are related to barrier heights. Bond dissociation energies are also determined, highlighting TMP's susceptibility to various reaction pathways. The discussion and findings elucidate the need for further experimental validation for practical applications of TMP in chemical synthesis, combustion, flame-retardant technologies, environmental processes, and pharmaceutical research.

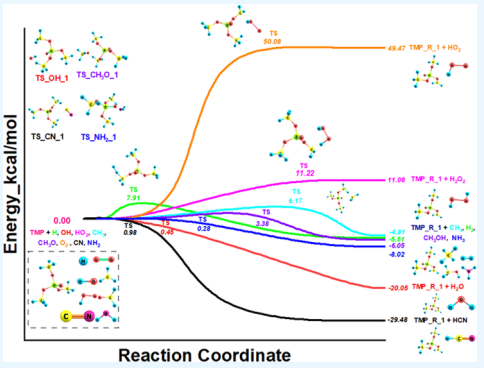

1. INTRODUCTION

Organophosphorus compounds[1,2] (OPCs) are classified into phosphonates,[3,4] phosphates,[5,6] phosphinates,[7] and phosphazenes.[8,9] They are used in various applications ranging from incineration[10] of pesticides and chemical warfare agents[11] to fire suppression[12] and potential catalytic uses in aircraft turbines or combustion technology.[13,14] Despite studies[1,15−17] involving OPCs in different applications, a complete understanding of their behavior remains elusive. Hence, the potential of phosphorus-containing compounds has sparked significant interest in their thermochemistry and reaction mechanisms for practical and effective applications.[18−21] Trimethyl phosphate[22−24] consists of a central phosphorus (P) atom double-bonded to an oxygen atom (O) and single-bonded to three methoxy (CH_3O) groups, as illustrated in Figure 1.

Exploring Trimethyl Phosphate's (TMP's) thermochemistry and rate kinetics properties provides insights into energy changes in reactions it participates in, reaction mechanisms, optimizing conditions, and achieving desired rates and yields.[25] TMP's significance spans chemical synthesis, process efficiency, and environmental impact assessment. For example, TMP's role in phosphorylating polymer[26] surfaces benefits from optimized reaction temperatures and reaction time adjustments guided by rate kinetics.[27] In polymers, TMP's flame-retardant function relies on reactivity and stability. This

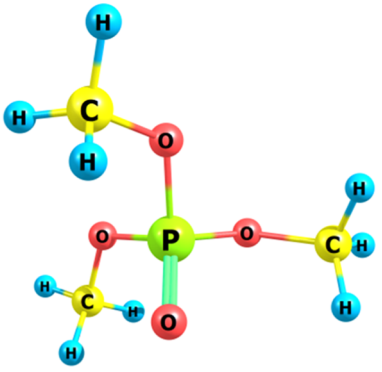

Figure 1. Geometry of TMP.

Received: September 18, 2023
Revised: November 8, 2023
Accepted: November 10, 2023
Published: December 4, 2023

understanding also assesses TMP's reactivity and stability under various conditions, crucial for safe handling and storage.[28−31]

Hydrogen atom abstraction reactions generate radicals, driving reaction mechanisms and forming diverse products relevant to combustion engines, atmospheric processes, and polymerization.[28,32,33] Established mechanisms underscore the role of hydrogen atom abstraction in initial reaction stages, contributing to the comprehensive understanding of these reactions.[34] Investigating TMP's behavior through hydrogen atom abstraction reactions[35] provides insights into its chemical reactivity. These reactions are pivotal in initiating radical chain reactions across various chemistry domains.[36,37] Various studies by Glaude,[10] Korobeinichev,[30,38−40] and Jayaweera[39] relating to H-atom abstractions have modeled parameters for Arrhenius equations, from which their rate constants are illustrated in Figure 2.

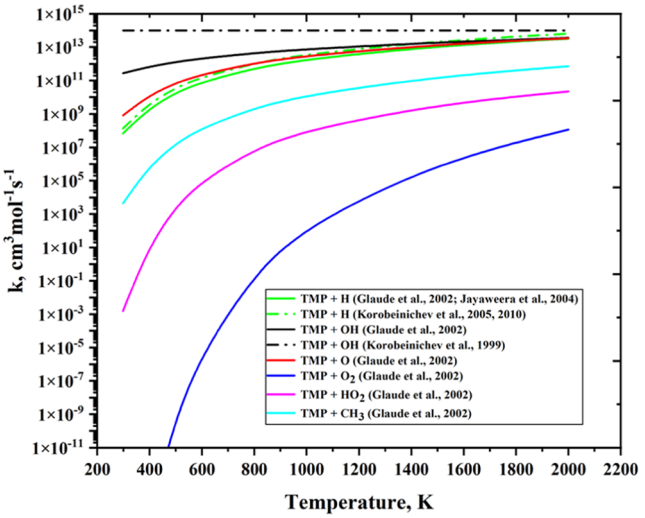

Figure 2. Currently available TMP H-atom abstraction reactions.

As illustrated in Figure 2, differences in calculated rates may arise due to the varied reaction mechanisms, intermediates, and transition states considered. Additionally, including or excluding specific reaction pathways, radical species, or molecular interactions affects overall kinetics and the calculated rates. The accuracy of quantum chemistry calculations[17] also plays a pivotal role, as slight variations in computational methods, basis sets, and levels of theory lead to differences in energy calculations and activation barriers. Rate discrepancies can also be attributed to differences in conditions, such as temperature and pressure. Reaction rates are sensitive to these factors, and slight adjustments can result in differing rate constant values.[41]

Rigorous approaches, such as experimental validation, benchmarking against dependable data, and employing high-level quantum chemistry calculations, allow the creation and optimization of reaction processes, guaranteeing safety, efficiency, and meticulous predictions across diverse applications.[42] Theoretical calculations predict reaction barriers and product distributions, uniting empirical observations with comprehension. Techniques like laser spectroscopy and mass spectrometry directly quantify these reactions, unveiling their pronounced reactivity and efficiency.[43]

This research explores TMP's thermochemistry and bond dissociation energies (BDE) through high-level ab initio quantum calculations, providing insights into its thermal stability. With a focus on H-atom abstraction (HAA) reactions, the kinetic intricacies of TMP are examined with its branching ratios and rates of its HAA reactions to address knowledge gaps and practical challenges, significantly enhancing fundamental understanding and practical applications across various domains.

2. THEORY AND METHODOLOGY

2.1. Computational Approach. The initial structure for TMP was obtained from the PubChem Database,[44] and the structure was optimized using the M06-2X/6-311++G(d,p) level of theory with Gaussian16 RevB.01 software.[45,46] All electronic structure calculations used the Gaussian 16 (Gaussian16 RevB.01) quantum mechanical packages.[47] With high-level ab initio calculations, geometries, vibration frequency, and dihedral scans for the lower-frequency modes, the internal rotations corresponding to low-frequency torsional modes were scanned in 10° increments as a function of the dihedral angle of TMP. All essential species (TMP and related radicals) were optimized at the M06-2X method[48] with the 6-311++G(d,p) basis set.[37,49]

The thermochemistry of the TMP and its three radical products were studied using the MultiWell[50] program suite.[51] These species' thermodynamic and kinetic properties of interest can be used for other extensive TMP studies (kinetic modeling and experiments). The MultiWell program suite performs kinetic calculations, employing statistical thermodynamics and rate theories for thermochemistry[52] data and rate constants. Subsequently, rate constants ranging from 298.15 to 2000 K for H-atom abstraction from different molecules have been performed using conventional transition state theory with asymmetric tunneling corrections.[53,54]

Vibrational frequency analysis determines the compounds' local minima or first-order saddle point character. The hindered rotation treatments for lower-frequency modes are carried out to confirm each species and transition states with a global minimum energy structure related to the C−H, O−P, and C−O single bonds in TMP. The vibrational frequencies, dihedral scans of optimized geometries, and the enthalpies of formation at 0 K obtained by the methods listed in Supporting Information Table S1 are input to the MultiWell program suite. The mass, moment of inertia, and electronic multiplicities obtained from quantum chemistry calculations were utilized to determine the partition functions for the reactants, products, and transition states. All zero point energies (ZPE) and vibrational frequencies[55−57] were scaled by 0.983 and 0.9698, respectively, as recommended for the M06-2X functional by Zhao and Truhlar.[48] The M06-2X method with the 6-311++G(d,p) basis set was also used to obtain the intrinsic reaction coordinate (IRC) calculations to ensure that each transition state (TS) is connected to the desired reactants and products.

The Lamm module within the Multiwell Suite calculated the external rotational constants. It reduced the moment of inertia for hindered internal rotations. In the rate constant calculations, quantum mechanical tunneling was considered for an unsymmetrical Eckart barrier model. The Thermo module within the Multiwell Suite is used to compute thermodynamic functions and high-pressure limiting rate constants based on transition state theory (TST). Then, the

https://doi.org/10.1021/acsomega.3c07137
ACS Omega 2023, 8, 47134−47145

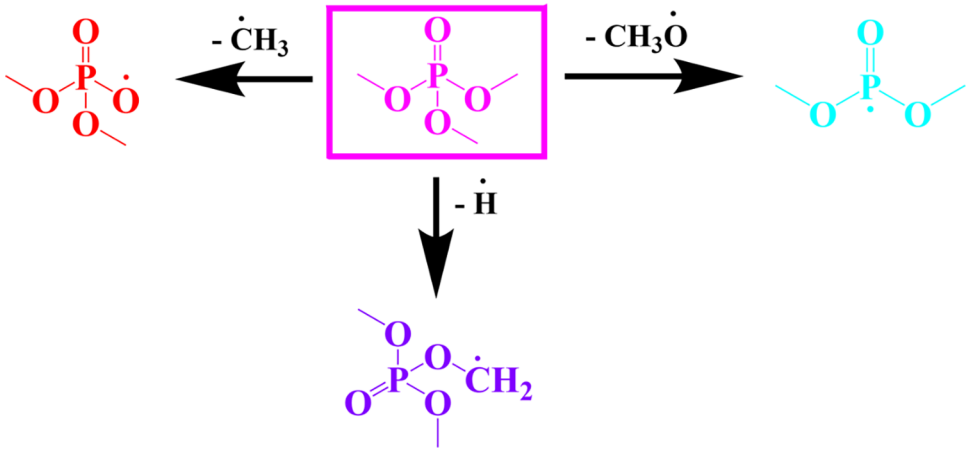

Figure 3. Bond dissociation energy (BDE) of TMP.

calculated rate constants are fitted to a modified temperature-dependent Arrhenius expression illustrated as eq 1

$$k = A(T)^n \exp\left(-\frac{E}{RT}\right) \quad (1)$$

where A is the frequency factor, T is the temperature in Kelvin, n is the temperature exponent at 1 K, and E is related to the activation energy, as shown in eq 2

$$E_a = E + nRT \quad (2)$$

The atomization method determines all species' necessary thermodynamic data using the average composite methods of CBS-APNO, G3,[58] G4,[59] CBS-QB3, G3B3,[58,60] and G2.[61] Single point energies (SPE) are calculated by using coupled-cluster theory CCSD/cc-pVXZ (where X = D and T) and Møller−Plesset perturbation theory MP2/cc-pVXZ (where X = D, T, and Q), The resulting SPEs were extrapolated to the complete basis set (CBS) limit using eq 3[55]

$$\begin{aligned} &E_{\mathrm{CCSD/cc\text{-}pVTZ}} + (E_{\mathrm{CCSD/cc\text{-}pVTZ}} - E_{\mathrm{CCSD/cc\text{-}pVDZ}})^* 3^4 \\ &/(4^4 - 3^4) + E_{\mathrm{MP2/cc-pVQZ}} \\ &+ (E_{\mathrm{MP2/cc-pVQZ}} - E_{\mathrm{MP2/cc\text{-}pVTZ}})^* 4^4/(5^4 - 4^4) \\ &- E_{\mathrm{MP2/cc\text{-}pVTZ}} + (E_{\mathrm{MP2/cc\text{-}pVTZ}} - E_{\mathrm{Q/cc\text{-}pVDZ}})^* 3^4 \\ &/(4^4 - 3^4) \end{aligned} \quad (3)$$

The Master Equation System Solver (MESS) package[62] via the eigenvalue method was used to evaluate temperature- and pressure-dependent rate coefficients for fine-tuning rates or reactions. The MESS package was used to solve the one-dimensional (1-D) master equation and to compute temperature-dependent phenomenological rate constants in the zero and high-pressure limits within the Rice−Rampsberger−Kassel−Marcus (RRKM) Master Equation theory.[63] The rigid-rotor harmonic oscillator (RRHO) model was used to compute densities of states and partition functions of local minima and number of transition states.

2.2. Conformer Search. Trimethyl phosphate (TMP) exhibits diverse three-dimensional conformations due to bond rotations and other factors. These different conformations influence reactivity, impacting reaction mechanisms and product outcomes. Each TMP conformation has unique thermodynamic properties, aiding stability assessments under varying conditions. This knowledge is valuable for predicting the behavior of TMP at different temperatures and pressures and its interactions with solvents. Understanding various conformers is essential for comprehending TMP's behavior in solutions, which is crucial in chemical, environmental, and industrial processes. Identifying conformational changes is significant for predicting precise reaction pathways and outcomes.

The optimized-M06-2X TMP structure was subjected to the systematic conformer search algorithm in Spartan'14 software, Version 1.1.4,[64] to generate TMP conformers under five levels of theories. A sixth level of theory was also used for the Conformer searches of TMP via the Entos-Envision software.[65] In our study, using six levels of theory in various computational methods led to different numbers of conformers, each with its own set of parameters and approximations.

In a general scheme of work, conformers with minimal relative energy are ideal for further investigation, hence the relevance of higher-level theory in determining the number of conformers based on the chosen algorithms and search methods. However, the M06-2X/6-311++G(d,p) Optimized TMP Structure subjected to a Dihedral Scan was used for all calculations. The conformer search was not the primary focus of this study; as related, previous studies[23,24,66] have emphasized its significance and the precise number of TMP conformers.

2.3. Bond Dissociation Energies (BDEs). The BDEs of TMP provide essential insights into TMP's reactivity and can vary depending on the type of broken bond. Evaluating the various single-bond dissociation energies in TMP, the atomization methods give three calculations, as illustrated in Figure 3.

This study explored two approaches for calculating the bond energies: Total Energy at Zero Kelvin (TEZK) and Standard Enthalpy of Formation (SEF) methods. TEZK, which seeks to express the total electronic energy of a molecule at 0 K, caused by low-frequency mode vibrations, is the total of the correction factor (zero point energy (ZPE)) and the single point energy (SPE) of the molecule.

2.3.1. Total Energy at Kelvin Energy (TEZK) Method. This method is developed from the analogy of enthalpy of atomization, where the atomization method is deduced as shown in eqs 4−8

$$C_3H_9O_4P(\mathrm{TMP}) \rightarrow 3C + 9H + 4O + 1P \quad (4)$$

https://doi.org/10.1021/acsomega.3c07137
ACS Omega 2023, 8, 47134−47145

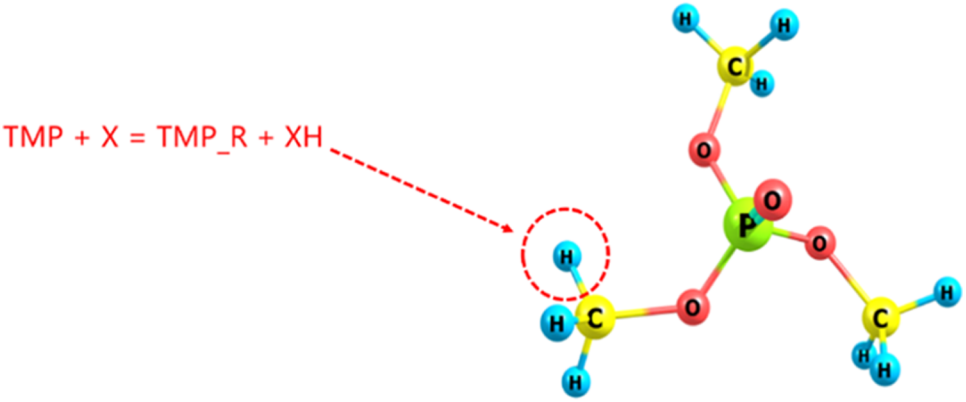

Figure 4. H-atom abstraction of TMP.

$$(\mathrm{TAE_0})\text{of TMP} = 3\mathrm{H_0(C)} + 9\mathrm{H_0}(H) + 4\mathrm{H_0(O)} + \mathrm{H_0}(P) - \mathrm{H_0}(C_3H_9O_4P) \quad (5)$$

$$\Delta_f\mathrm{H_0(TMP)} = 3\Delta_f\mathrm{H_0}(\mathrm{C_3}) + 9\Delta_f\mathrm{H_0}(\mathrm{H_9}) + 4\Delta_f\mathrm{H_0}(\mathrm{O_4}) + 1\Delta_f\mathrm{H_0}(\mathrm{P_1}) - (\mathrm{TAE_0}) \quad (6)$$

where $(\mathrm{TAE_0})$ denotes total atomization energy. The TEZK for BDE calculations of TMP was calculated using eq 7

$$\mathrm{TEZK(TMP)} = \mathrm{TEZK(sum\ of\ the\ products)} - \mathrm{TEZK(reactants)} \quad (7)$$

$$\mathrm{TEZK(TMP)} = \mathrm{TEZK}(B + C) - \mathrm{TEZK}(A) \quad (8)$$

$$\mathrm{BDE(TMP)} = \mathrm{TEZK(TMP)} \times \mathrm{au(in\ kcal/mol)} \quad (9)$$

where 1 au (atomic unit) = 627.5095 kcal/mol, *A* is TMP, and *B* and *C* are the radicals formed after dissociating every single bond within TMP, as illustrated in Figure 3.

2.3.2. Standard Enthalpy of Formation (SEF) Method. The second approach calculates BDE, as shown in eq 10

$$\mathrm{BDE} = \Delta_r\mathrm{H_{298.15K}} = [\Delta_f\mathrm{H_{298.15K}}(B) + \Delta_f\mathrm{H_{298.15K}}(C)] - \Delta_f\mathrm{H_{298.15K}}(A) \quad (10)$$

where *A* is TMP, and *B* and *C* are the radicals formed after dissociating each single bond within TMP, as illustrated in Figure 3. The main difference between the TEZK and SEF method is that the values obtained via the TEZK method are from the combined methods of atomization (CBS-APNO/G3/G4/G3B3/G2/CBS-QB3) energy estimation at 0 K. In comparison, the SEF method uses the values obtained at 298.15 K.

2.4. H-Atom Abstraction Reactions (HAA). In verifying the combustion chemistry of TMP, eight H-atom abstraction reactions were systematically studied. This study abstracts an H atom from a methyl group in TMP, as illustrated in Figure 4, with stable species, O_2 (oxygen), H (hydrogen) and radicals [$\dot{O}H$ (hydroxyl), $\dot{C}H_3$ (methyl), $CH_3\dot{O}$ (methoxy), $H\dot{O}_2$ (hydroperoxyl), NH_2 (amino), and CN (cyano), $\dot{N}H_2$ (amino), and $\dot{C}N$ (cyano)]. The transition states corresponding to these reactions reveal the transition from reactants to products, with detailed geometrical parameters capturing the crucial bond-breaking and bond-forming processes. Such insight into the transition states is essential for understanding the activation barriers that dictate the reaction kinetics.

The details of TMP H-atom abstractions are summarized in Supporting Information Table S2. Supporting Information Table S20 also highlights more information in the glossary of these species.

2.5. Branching Ratios. The branching ratios of a reaction pathway describe the relative probabilities that the reactants will follow different reaction paths, leading to the formation of other products. The branching ratio of TMP is the ratio of the formation rate of a particular intermediate to the formation rate of all intermediates combined. These ratios can provide valuable insights into the reaction pathways and the relative importance of different reaction channels. Analyzing favored products from branching ratios under specific conditions proposes consistent mechanisms with data on reaction pathways for mechanism development. Some products are kinetically favored due to lower activation barriers; others are thermodynamically favored due to lower energy states. This study analyzed the branching ratios from the rate constants estimated from Multiwell and MESS methods.

3. RESULTS AND DISCUSSION

3.1. Conformer Search and Dihedral Angle Scan. Relative energies per conformer indicate the stability within the molecule. Comparing these values across methods reveals trends in conformer stability predictions for more insight into the TMP behavior. The provided data in Supporting Information Tables S14−S19 highlight various conformer properties computed using different methods and basis sets, as well as other properties, including relative energies, highest occupied molecular orbital energy (E HOMO), lowest unoccupied molecular orbital energy (L HOMO), dipole moment, and Boltzmann constants from these methods. Several studies about TMP conformer searches have attributed the formation of conformers along various rotational and vibrational axes of TMP. From Supporting Information Figure S1, the conformers found are of a minimum of 5 to a maximum of 11 based on various methods. These discrepancies generated from various conformers with various relative energies further confirm the need for in-depth studies on how conformers' knowledge could affect the entire mechanistic insight of TMP.

To highlight an example of the results of the conformer search and with the results from Supporting Information, Table S14, which has the highest level of theory (M06/6-

https://doi.org/10.1021/acsomega.3c07137
ACS Omega 2023, 8, 47134−47145

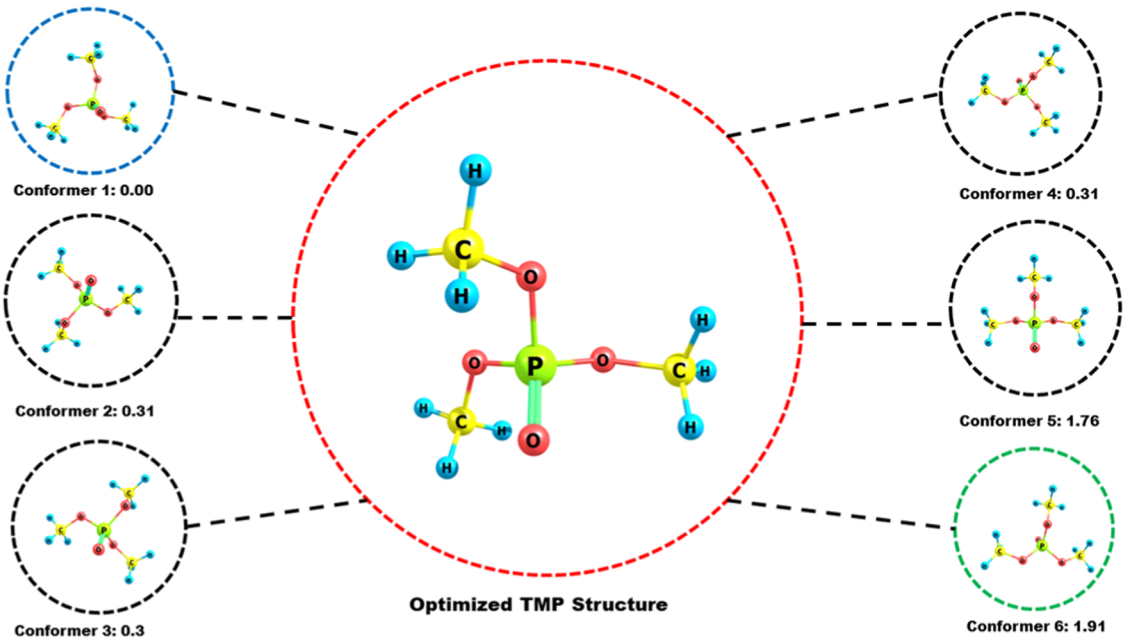

Figure 5. TMP conformers from the M06/6-311+G** level of theory.

Table 1. TMP Bond Dissociation Energies (BDE) and Bond Dissociation Free Energies (BDFE) in kcal/mol

bond type	current study, BDE (TEZK) method)	current study, BDE (SEF method)	ALFABET, BDE (ML prediction)[67]	ALFABET, BDE (DFT)[67]	owens[68]	ALFABET, BDFE, (ML prediction)[67]	ALFABET, BDFE (DFT)[67]
C−H	96.03	104.89	99.1	99.3	N/A	90.7	90.7
C−O	93.22	99.48	94.9	95.2	83.02	81.9	82.6
O−P	116.02	117.31	113.1	113.2	93.63	99.5	99.8

311+G**) used in the Conformer Search of this study within the Spartan'14 software, Version 1.1.4, Figure 5 illustrates the results.

Supporting Information Figure S1 summarizes the results of the dihedral scans of all single bonds within the optimized TMP molecule. Using the energy as a basis for comparison, it is observed that the energy levels along the C−O bonds connected by a methyl (CH_3) rotor are lower than those along the O−P bonds connected by a methoxy (CH_3O) rotor. By focusing on conformers that favor specific relevant orientations, evidence for particular reaction pathways or transition states emerges for developing detailed and extensive TMP mechanisms.

3.2. Bond Dissociation Energy. The results of the Total Energy at Zero Kelvin (TEZK) method used in calculating the bond dissociation energies within the TMP molecule are summarized in Supporting Information Table S3. Supporting Information Table S11 provides the individual energies obtained from CBS-APNO, G3, G4, G3B3, G2, and CBS-QB3 energy calculations that were used in the Total Energy at Zero Kelvin (TEZK)-Bond Dissociation Energy approach. Using the Standard Enthalpy of Formation (SEF) approach, the various bond dissociation energies within the TMP molecule are also summarized in Supporting Information Table S4. Table 1 compares this study's calculated BDEs with those of other available literature data.

The C−H, C−O, and O−P bonds uphold TMP's structural integrity. This stability has implications for the role of TMP in chemical reactions, suggesting that breaking these bonds requires substantial energy inputs. From Table 1, it can be concluded that generally, the C−O bond shows the lowest bond dissociation energy ranging from 83.02 to 99.48 kcal/mol, followed by the C−H bond ranging from 96.03 to 104.89 kcal/mol and then the O−P bond with the highest energy ranging from 93.63 to 117.31 kcal/mol. The bond dissociation energies, from the weakest to most substantial bonds, as shown in Figure 6, are the C−H bonds within the CH_3 (methyl) rotor

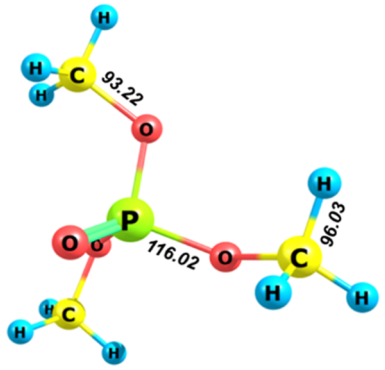

Figure 6. Bond dissociation energies of TMP in kcal/mol (obtained from the TEZK method).

group, the C−O bond within the CH_3O (methoxyl) group, and the O−P bond within the CH_3OP-group. The O−P bond possesses a BDE higher than that of the carbon-based bonds. This indicates the strength of the oxygen−phosphorus linkage, which plays a crucial role in the TMP's reactivity and function in various chemical processes.

3.3. Thermochemistry. The standard heat of formation, entropy, and specific heat capacities calculated for TMP and

https://doi.org/10.1021/acsomega.3c07137
ACS Omega 2023, 8, 47134−47145

Table 2. Estimated Thermochemistry Values for TMP and Relevant Species

reference (method)	species	ΔH_f° (kcal mol^{-1}), 298 K	S (cal mol^{-1} K^{-1}) 298 K	c_p (cal mol^{-1} K^{-1}) 300	400	500	600	800	1000	1500
Glaude et al.,[10]	TMP ($C_3H_9O_4P$)	−246.93	106.91	34.41	45.82	50.69	60.62	70.63	75.42	78.18
Neupane et al. (group additivity method)[69]	TMP ($C_3H_9O_4P$)	−254.84	106.99	36.64	47.14	51.80	61.78	71.95	76.90	80.65
current study (composite method of CBS-QB3, G3, G3B3 and G2)	TMP ($C_3H_9O_4P$)	−254.95	107.29	38.24	44.26	49.93	54.88	62.83	68.81	78.18
Khalfa et al., (group contributions)[17]	TMP ($C_3H_9O_4P$)	−254.55	106.29	37.80	44.53	50.74	56.05	64.39	70.54	N/A
Khalfa et al., (CBS-QB3 level of theory)[17]	TMP ($C_3H_9O_4P$)	−254.81	106.98	36.87	43.76	49.95	55.17	63.26	69.21	78.45
Glaude et al.,[10]	TMP_R_1 ($C_3\bar{H}_8O_4P$)	−198.32	109.01	38.87	43.39	47.24	50.65	56.53	61.55	71.94
Neupane et al., (group additivity method)[69]	TMP_R_1 ($C_3\bar{H}_8O_4P$)	−205.22	111.85	38.84	43.33	49.50	53.55	59.94	64.90	73.91
current study (composite method of CBS-QB3, G3, G3B3 and G2)	TMP_R_1 ($C_3\bar{H}_8O_4P$)	−202.16	114.02	38.01	43.35	48.42	52.85	59.93	65.24	73.58
Glaude et al.,[10]	TMP_BDE_R2 ($C_2\bar{H}_6O_4P$)	−185.72	97.41	32.93	36.74	40.00	42.88	47.84	52.08	60.77
Neupane et al., (group additivity method)[69]	TMP_BDE_R2 ($C_2\bar{H}_6O_4P$)	−199.03	95.26	32.04	36.10	40.53	44.18	49.95	54.43	62.56
current study (composite method of CBS-QB3, G3, G3B3 and G2)	TMP_BDE_R2 ($C_2\bar{H}_6O_4P$)	−190.48	98.52	32.63	36.20	40.03	43.56	49.31	53.61	60.28
Glaude et al.,[10]	TMP_BDE_R3 ($C_2\bar{H}_6O_3P$)	−137.51	93.00	26.71	32.09	36.26	39.67	45.05	49.22	56.81
Neupane et al., (group additivity method)[69]	TMP_BDE_R3 ($C_2\bar{H}_6O_3P$)	−147.00	92.40	26.36	31.80	36.03	39.48	44.93	49.16	56.84
current study (composite method of CBS-QB3, G3, G3B3 and G2)	TMP_BDE_R3 ($C_2\bar{H}_6O_3P$)	−142.79	94.55	25.93	30.31	34.50	38.13	43.85	48.07	58.92

other related species from this study and other available literature are listed in Table 2. The T1 diagnostic value from CCSD (T) and SPE calculations evaluate the uncertainties caused by the species' multireference effects and transition states. Generally, T1 diagnostic values for all radical species is ≤0.03, for all closed-shell molecules is ≤0.02, and for all of the transition states is ≤0.04, respectively. The T1 diagnostic values for TMP and related species, as shown in Table S20, Supporting Information, match high levels of accuracy.

3.4. Energy Barrier Comparisons. The potential energy diagram for the eight TMP H-atom abstractions with energy barrier comparisons can be visualized in Figure 7.

From Figure 7, the increasing order of magnitude barrier heights are $\dot{C}N$, $\dot{O}H$, $\dot{N}H_2$, $CH_3\dot{O}$, H, $\dot{C}H_3$, $H\dot{O}_2$, and O_2.

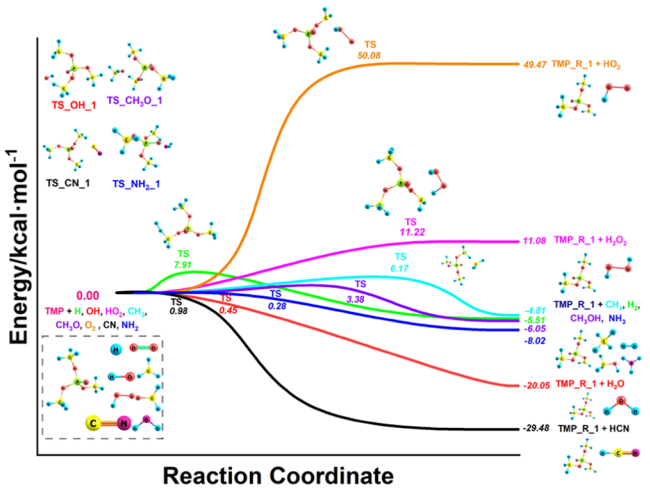

Figure 7. Potential energy diagram of TMP H-atom abstraction.

Supporting Information Table S5 summarizes the results of the forward and reverse energy barrier heights. Notably, the forward barrier heights range from 0.28 to 50.08 kcal/mol, indicating a broad spectrum of reactivity. Reactions involving TMP with $\dot{O}H$, $\dot{C}N$, and $\dot{N}H_2$ radicals exhibit significantly lower forward barrier heights, implying that these reactions are relatively fast and easy to achieve.

In contrast, reactions with H, $\dot{C}H_3$, $CH_3\dot{O}$, and $H\dot{O}_2$ radicals require higher energy inputs. The reverse barrier heights demonstrate varying trends. While reactions with $\dot{O}H$ and $H\dot{O}_2$ radicals have remarkably low reverse barrier heights, implying more accessible backward reactions, reactions involving TMP with $\dot{C}N$ and O_2 exhibit notably high reverse barrier heights. This discrepancy suggests that the reversibility of these reactions is highly dependent on the nature of the reacting species.

3.5. Rate Constant Calculations. In this study, two different methods, Multiwell and MESS, were used to determine the rate constants of the HAA reactions. Supporting Information Tables S6 summarizes the results of TMP H-Atom Abstraction obtained in this study for the Arrhenius equation stated in eq 1, comparing with two methods of Multiwell and MESS, providing critical insights into the kinetics of TMP's H-atom abstraction reactions using the Arrhenius equation parameters from eq 1. The pre-exponential factor (A), which quantifies the collision frequency, ranges from 0.032 to 190,700 s^{-1}. This broad range signifies the varied likelihood of successful collisions, leading to reaction initiation. Activation energy (E_a) values, which dictate the energy barrier for the reaction, span from −2.896 to 49.324 kcal/mol. Higher E_a values correspond to reactions with higher energy barriers, indicating slower kinetics. Notably, the reaction involving TMP with O_2 exhibits a particularly high E_a value, suggesting

https://doi.org/10.1021/acsomega.3c07137
ACS Omega 2023, 8, 47134−47145

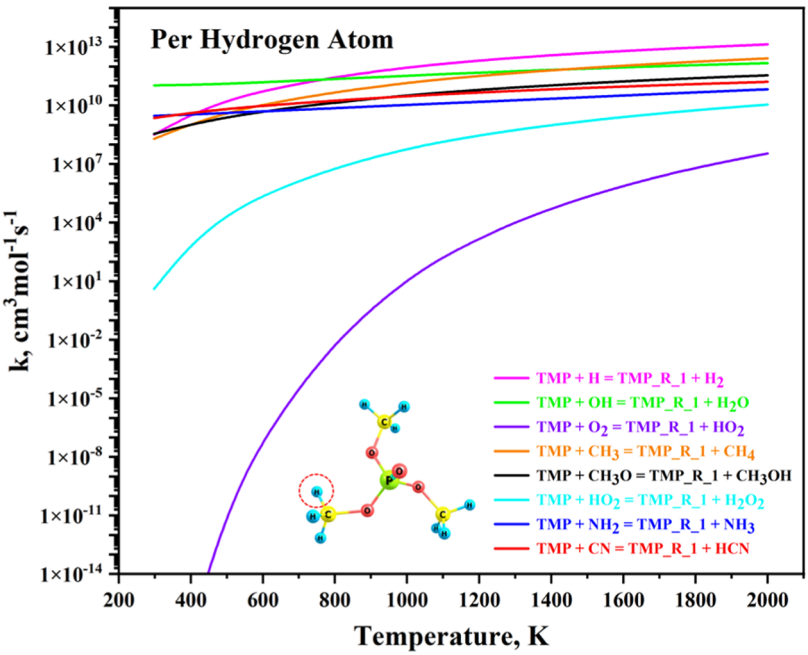

Figure 8. Rates of TMP H-atom abstraction.

that this reaction is energy-intensive and likely kinetically hindered.

The theoretical rates obtained from the Multiwell method of the H-atom abstraction reactions, as illustrated in Figure 8, confirm the barrier height analyses, with reactions of H and ȮH radicals being the fastest reaction and O_2 being the slowest. At lower temperatures, ȮH has the fastest rate; however, around 800 K, the reaction rate for H becomes the fastest. The general rate trend for all of the abstractions at higher temperatures tends to converge.

3.5.1. Further HAA Rates Comparison. Available studies concerning TMP H-atom abstraction are compared with the calculated rates in this study. Most studies show trends and rates similar to those of the TMP + H reaction, as illustrated in Figure 9. However, the current study rate calculated with the Multiwell method differs with a higher rate across all illustrated temperature ranges.

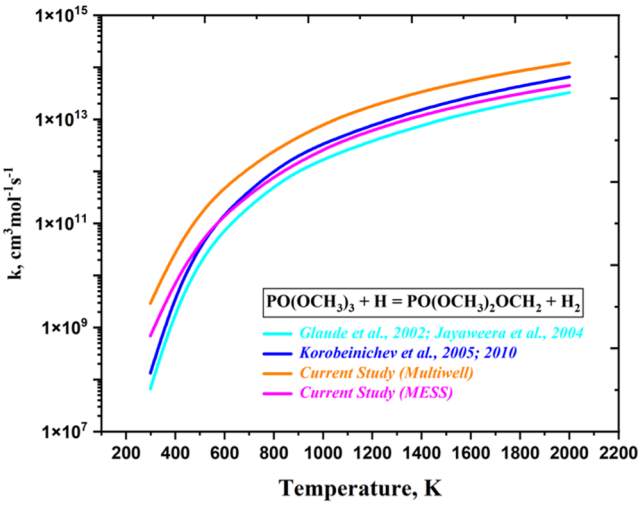

Figure 9. Comparison of the TMP + H abstraction reactions.

TMP + ȮH, O_2, and HȮ$_2$ reactions are crucial in atmospheric chemistry, affecting pollutant degradation and ozone depletion. Hence, the need for accurate calculated rates involving these reactions aids in such fields of study. With the TMP + OH reaction, as illustrated in Figure 10, most studies

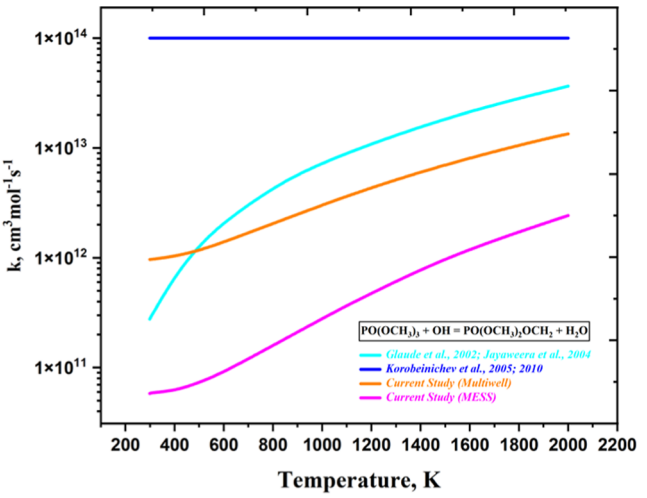

Figure 10. Comparison of the TMP + ȮH abstraction reactions.

differ from the current rates calculated. The trend, however, is a general increase in rates with increasing temperature. However, the study by Korobeinichev et al.[30,38] shows quite a different trend, which could be attributed to analogies and estimations instead of rate determination by calculations.

With the TMP + O_2 reaction, as illustrated in Figure 11, all previous studies are similar to the calculated rates in this study.

With the TMP + HȮ$_2$ reaction, as illustrated in Figure 12, Glaude et al.'s[10] study differs by several orders of magnitude compared to the calculated rates in this study.

https://doi.org/10.1021/acsomega.3c07137
ACS Omega 2023, 8, 47134−47145

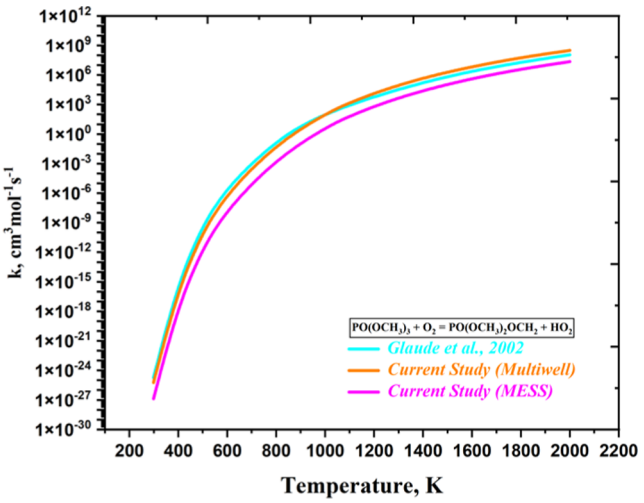

Figure 11. Comparison of TMP + O_2 abstraction reactions.

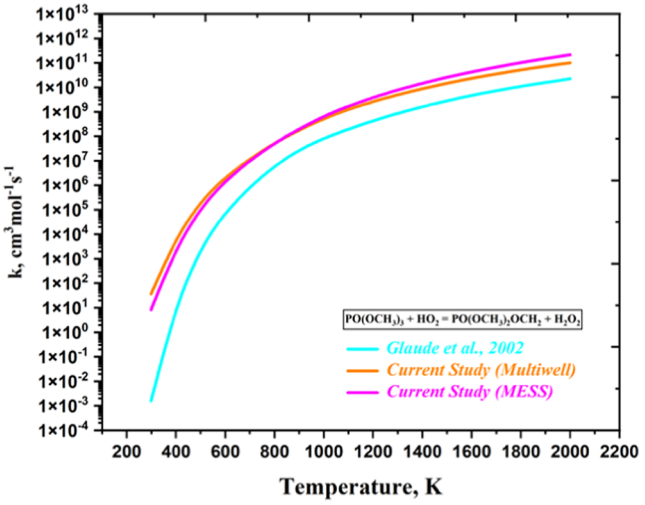

Figure 12. Comparison of the TMP + $H\dot{O}_2$ abstraction reactions.

With the TMP + $\dot{C}H_3$ reaction, as illustrated in Figure 13, Glaude et al.'s[10] study differs by several orders of magnitude at lower temperatures but converges at higher temperatures.

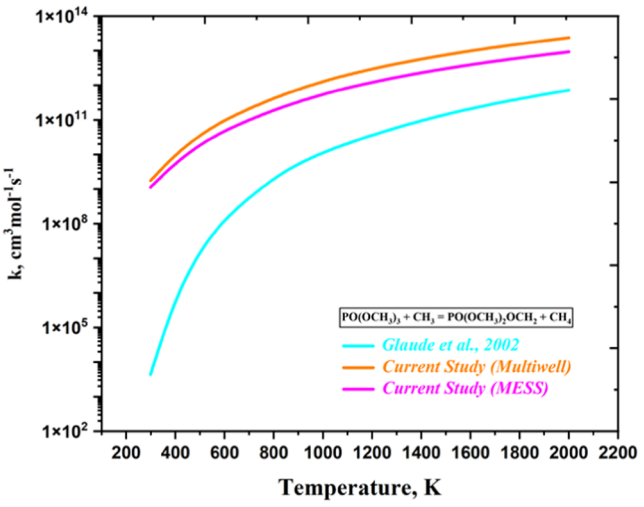

Figure 13. Comparison of TMP + $\dot{C}H_3$ abstraction reactions.

With no available literature study data on the TMP + $CH_3\dot{O}$ reaction, the estimated rates, as calculated in this study and illustrated in Figure 14, slightly differ at lower temperatures and tend to diverge at higher temperatures.

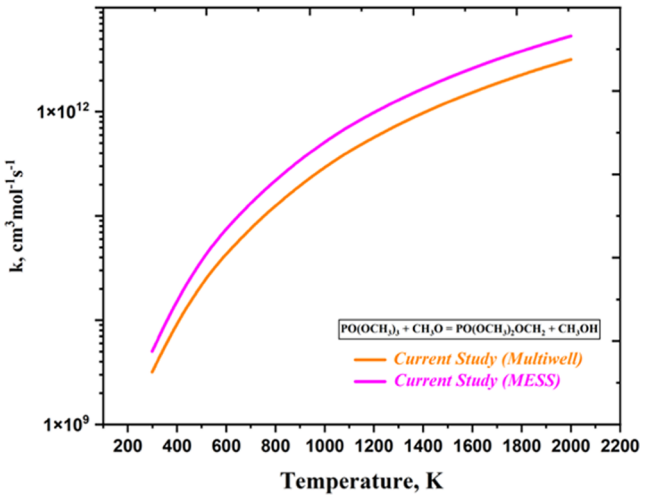

Figure 14. Comparison of the TMP + $CH_3\dot{O}$ abstraction reactions.

With TMP + $\dot{C}N$ and TMP + $\dot{N}H_2$ reactions, Figure 15 shows a significant disparity between the rates calculated by

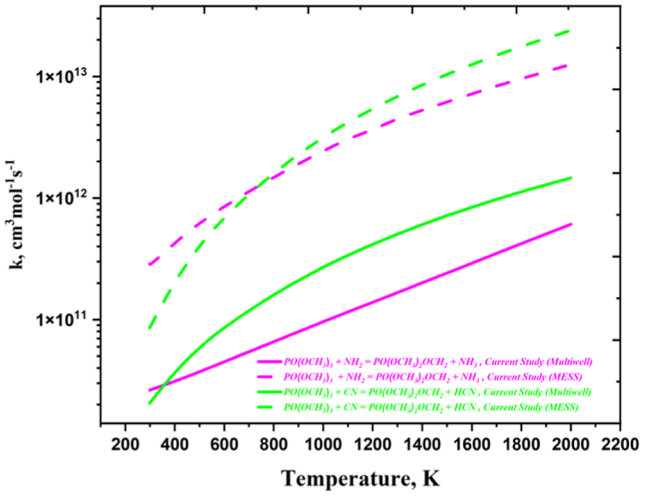

Figure 15. Comparison of TMP + $\dot{N}H_2$ and TMP + $\dot{C}N$ abstraction reactions.

the Multiwell method and MESS. This observation emphasizes the need for a very accurate rate calculation to understand the behavior of the TMP mechanism.

3.5.2. Critical Assessment on TMP + ȮH Reaction. Minimal data are currently available for studies on Trimethyl phosphate that accurately validate a complete kinetic model. Figure 16 highlights the experimental data for the TMP + ȮH reaction to form water and other species. As illustrated in Figure 16 and the available literature, there seems to be a negative temperature dependence in the lower range of temperatures. In the work done by Koshlyakov et al.,[70] the experimental data obtained between 273 and 873 K was then fitted to estimate the rates at other conditions. Tuazon et al.[71] measured the rate at 296 K, and Aschmann et al.[72] re-evaluated the rate at 296 K with an indirect measurement method. Burns

https://doi.org/10.1021/acsomega.3c07137
ACS Omega 2023, 8, 47134−47145

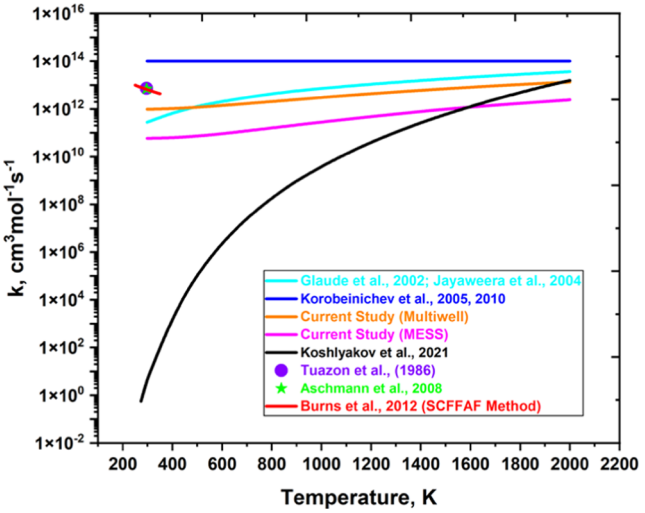

Figure 16. TMP + ȮH reactions.

et al.[73] also made estimations between the temperature of 250−350 K. Various reasons arise to explain the different trends observed in Figure 16, such as the formation of other intermediates species, van der Waals (VDW) complexes, and transition states. The products, however, and the influence of other reactions are needed to explain the TMP + ȮH decomposition and abstraction reactions fully.

3.6. Branching Ratios. As illustrated in Figure 17, the high ȮH and H branching ratios at lower temperatures for TMP H-

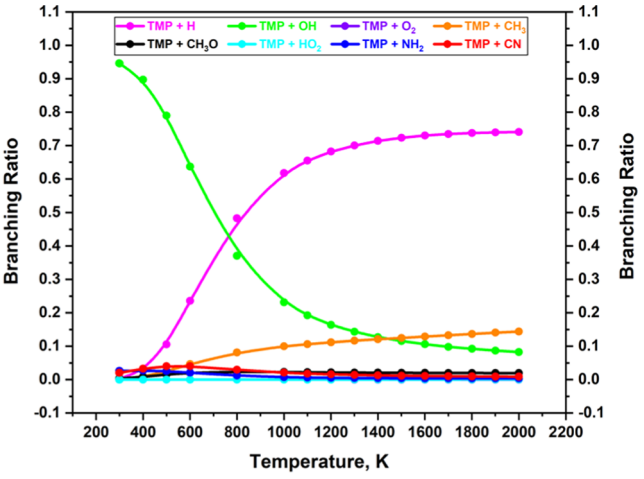

Figure 17. TMP HAA branching ratios of rates calculated with the Multiwell method.

atom abstraction reactions suggest that the formation of TMP−ȮH and TMP−H intermediates is favored. The high branching ratios of these reactions also indicate that they are more dominant pathways for TMP decomposition, resulting in the formation of fewer radical species that can promote combustion. TMP−ȮH and TMP−H intermediates will likely undergo further reactions that lead to the formation of stable, non-reactive species, such as water and methyl radicals, which can act as flame inhibitors by consuming free radicals that promote chain reactions in the combustion process. These radicals are known to be involved in the propagation steps of combustion reactions.

The branching ratios in Figure 18 highlight the need for accurately determining rate constants, as the rates obtained via

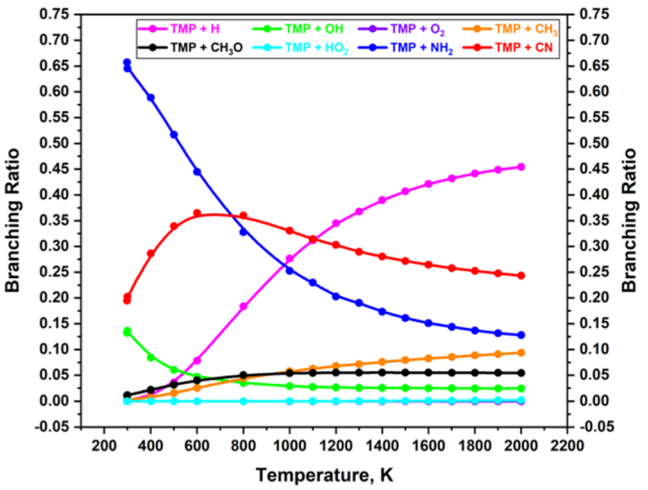

Figure 18. TMP HAA branching ratios of rates calculated with the MESS method.

Multiwell show variation from those obtained by MESS. However, the general trends validate that H and ȮH reactions are essential.

4. CONCLUSIONS

Trimethyl Phosphate has varied applications in battery safety, thermal stability, and flame retardancy. This study uniquely explores TMP's intricate realm, unveiling its H-atom abstraction reaction thermochemistry and rate kinetics. Calculated BDEs, reaction barriers, and rate constants offer quantitative insights, guiding the TMP's reactivity across chemical contexts. A theoretical analysis employing eight H-atom abstraction (HAA) reactions through high-level quantum chemical calculations validates TMP's combustion chemistry and kinetics. This encompasses rate constants, potential energy surface graphs, and branching ratios of the HAA reactions.

The study employs high-level ab initio quantum chemistry calculations to probe TMP's thermochemistry and that of other species. It utilizes Multiwell and MESS solver methods to investigate the reaction kinetics and rate constants for various H-atom abstraction reactions of TMP. The investigation into TMP's H-atom abstraction reactions elucidated various mechanisms and pathways. The impact of substituents and reaction conditions highlighted the intricate interplay between structural factors and external influences in steering the reaction selectivity. This understanding enriches our understanding of the TMP's reactivity. It holds implications for rationalizing and predicting the behavior of similar molecules in various chemical processes. These techniques determine rate constants, elucidating relevant pathways and constants for TMP-related reactions in combustion. This aids combustion efficiency, emissions reduction, and energy optimization studies applicable in industries ranging from automotive and aerospace to energy production.

Within TMP's molecule, the evaluation of bond dissociation energies (BDE) emphasizes the C−O bond with the lowest bond dissociation energy ranging from 83.02 to 99.48 kcal/mol, followed by the C−H bond ranging from 96.03 to 104.89 kcal/mol and the O−P bond with the highest energy ranging from 93.63 to 117.31 kcal/mol. The concept of bond

https://doi.org/10.1021/acsomega.3c07137
ACS Omega 2023, 8, 47134−47145

dissociation energies could further explore the O−P double bonds in future studies.

Pathway and rate constant knowledge shape novel catalysts, selectively promoting desired H-atom abstractions, yielding higher yields, purity, and fewer byproducts in syntheses. This study's comprehensive analysis underscores TMP's high reactivity, particularly in hydrogen atom abstraction reactions, which are initial steps in various pathways and are temperature-dependent. It also enriches the understanding of TMP's chemistry, with implications for fundamental research and practical applications in addressing environmental concerns about air quality and climate change and propelling more efficient combustion system development, fuel, and engine design.

■ ASSOCIATED CONTENT

Supporting Information

The Supporting Information is available free of charge at https://pubs.acs.org/doi/10.1021/acsomega.3c07137.

Quantum calculation methods used in this study for conformer search and estimation of thermochemistry properties of TMP; species involved in the TMP HAA reactions with related barrier heights, bond dissociation energies data, and tables that show the estimated TMP H-atom abstraction parameters for the Arrhenius equation (Part 1); cartesian coordinates (XYZ format) of TMP and related radicals Cartesian optimized with the M06-2X level of theory (Part 2); NASA polynomials of TMP and related radical species calculated from this study and other specified literature sources (Part 3); summarizes data on the single point energies and uses Multiwell and MESS methods to rate kinetics data of TMP HAA reactions (Part 4); obtained data on the conformer search conducted with different levels of theories in this study (Part 5); glossary and T1 Diagnostics of TMP, Radicals, and Transition States (Part 6); geometry of all conformers (Part 7); and summarized data for critical TMP + ȮH Reaction assessment (Part 8) (ZIP)

■ AUTHOR INFORMATION

Corresponding Author

Yang Li − *National Key Laboratory of Solid Rocket Propulsion, School of Astronautics, Northwestern Polytechnical University, Xi'an 710072, China; Science and Technology on Combustion, Internal Flow and Thermostructure Laboratory, School of Astronautics, Northwestern Polytechnical University, Xi'an 710072, China; Shenzhen Research Institute of Northwestern Polytechnical University, Shenzhen 518057, China;* orcid.org/0009-0003-8844-9346; Email: yang.li@nwpu.edu.cn

Author

Frederick Nii Ofei Bruce − *National Key Laboratory of Solid Rocket Propulsion, School of Astronautics, Northwestern Polytechnical University, Xi'an 710072, China; Science and Technology on Combustion, Internal Flow and Thermostructure Laboratory, School of Astronautics, Northwestern Polytechnical University, Xi'an 710072, China; Shenzhen Research Institute of Northwestern Polytechnical University, Shenzhen 518057, China; Department of Computational Chemistry, Nesvard Institute of Molecular Sciences, Accra 00000, Ghana;* orcid.org/0000-0003-3928-3928

Complete contact information is available at: https://pubs.acs.org/10.1021/acsomega.3c07137

Author Contributions

F.N.O.B.: Quantum calculations, overall conceptualization of the study, graphical and tabular representations, writing—editing and revision. Y.L.: supervision and provision of financial resources for this project.

Funding

The authors acknowledge the funding support from the National Natural Science Found Projects of China (22375165), the Faculty Building Project-National Young Talent from Northwestern Polytechnical University (0602023GH0202278), the Startup Funds of Aoxiang Overseas Scholar from Northwestern Polytechnical University (0602021GH0201182), the Shenzhen Research Institute of Northwestern Polytechnical University and HPC computational resources from King Abdullah University of Science and Technology, KAUST (Shaheen) Cluster, provisioned under the auspices of Prof. Mani Sarathy.

Notes

The authors declare no competing financial interest.

■ ACKNOWLEDGMENTS

The authors acknowledge the funding support from National Natural Science Found Projects of China (22375165). The authors appreciate the technical assistance on various computational processes given by Bai Xin, Ren Xuan, Ruining He, and Prof. Yue Ma, all from Northwestern Polytechnical University. Great appreciation also goes to Ernest Opoku (Nesvard Institute of Molecular Sciences), Cecil H. Botchway (Kwame Nkrumah University of Science and Technology), Esther Chota (Chang'an University), and Sandra Asante (Xi'an Jiaotong University) for the insightful discussions on environmental sustainability.

■ REFERENCES

(1) Glaude, P. A.; Curran, H. J.; Pitz, W. J.; Westbrook, C. K. Kinetic Study Of The Combustion Of Organophosphorus Compounds. *Proc. Combust. Inst.* **2000**, *28* (2), 1749−1756.

(2) Delfino, R. T.; Ribeiro, T. S.; Figueroa-Villar, J. D. Organophosphorus Compounds as Chemical Warfare Agents: A Review. *J. Braz. Chem. Soc.* **2009**, *20* (3), 407−428.

(3) Shaw, S. D.; Blum, A.; Weber, R.; Kannan, K.; Rich, D.; Lucas, D.; Koshland, C. P.; Dobraca, D.; Hanson, S.; Birnbaum, L. S.; Shaw, S. Halogenated Flame Retardants: Do the Fire Safety Benefits Justify the Risks? *Rev. Environ. Health* **2010**, *25* (4), 261−306.

(4) Babrauskas, V.; Fuoco, R.; Blum, A. Flame Retardant Additives in Polymers: When Do the Fire Safety Benefits Outweigh the Toxicity Risks?. In *Polymer Green Flame Retardants*; Elsevier Inc., 2014; Chapter 3, pp 87−118.

(5) Qin, P.; Yi, D.; Xing, J.; Zhou, M.; Hao, J. Study on Flame Retardancy of Ammonium Polyphosphate/Montmorillonite Nanocompound Coated Cellulose Paper and Its Application as Surface Flame Retarded Treatment for Polypropylene. *J. Therm. Anal. Calorim.* **2021**, *146* (5), 2015−2025.

(6) Lim, K. S.; Bee, S. T.; Sin, L. T.; Tee, T. T.; Ratnam, C. T.; Hui, D.; Rahmat, A. R. A Review of Application of Ammonium Polyphosphate as Intumescent Flame Retardant in Thermoplastic Composites. *Composites, Part B* **2016**, *84*, 155−174.

(7) Montchamp, J. L. Phosphinate Chemistry in the 21st Century: A Viable Alternative to the Use of Phosphorus Trichloride in Organophosphorus Synthesis. *Acc. Chem. Res.* **2014**, *47* (1), 77−87.
(8) Zhou, X.; Qiu, S.; Mu, X.; Zhou, M.; Cai, W.; Song, L.; Xing, W.; Hu, Y. Polyphosphazenes-Based Flame Retardants: A Review. *Composites, Part B* **2020**, *202*, No. 108397, DOI: 10.1016/j.compositesb.2020.108397.
(9) Allcock, H. R.; Chen, C. Polyphosphazenes: Phosphorus in Inorganic-Organic Polymers. *J. Org. Chem.* **2020**, *85* (22), 14286−14297.
(10) Glaude, P. A.; Melius, C.; Pitz, W. J.; Westbrook, C. K. Detailed Chemical Kinetic Reaction Mechanisms For Incineration Of Organophosphorus And Fluoro-Organophosphorus Compounds. *Proc. Combust. Inst.* **2002**, *29*, 2469−2476.
(11) Lavoie, J.; Srinivasan, S.; Nagarajan, R. Using Cheminformatics to Find Simulants for Chemical Warfare Agents. *J. Hazard. Mater.* **2011**, *194*, 85−91.
(12) Babrauskas, V. *Ignition Handbook*; Fire Science Publishers, 2003.
(13) Babushok, V. I.; Linteris, G. T.; Meier, O. C. Combustion Properties of Halogenated Fire Suppressants. *Combust. Flame* **2012**, *159* (12), 3569−3575.
(14) Hastie, J. W.; Bonnell, D. W. *Molecular Chemistry of Inhibited Combustion Systems*, 1980.
(15) Neupane, S.; Peale, R.; Vasu, S. Infrared Absorption Cross Sections of Several Organo-Phosphorous Chemical-Weapon Simulants. *J. Mol. Spectrosc.* **2019**, *355*, 59−65.
(16) Dorofeeva, O. V.; Ryzhova, O. N.; Zverev, V. G. Computational Study of the Thermodynamic Properties of Organophosphorus(V) Compounds. *J. Mol. Struct.: THEOCHEM* **2007**, *811* (1−3), 267−279, DOI: 10.1016/j.theochem.2006.12.053.
(17) Khalfa, A.; Ferrari, M.; Fournet, R.; Sirjean, B.; Verdier, L.; Glaude, P. A. Quantum Chemical Study of the Thermochemical Properties of Organophosphorous Compounds. *J. Phys. Chem. A* **2015**, *119* (42), 10527−10539.
(18) Mackie, J. C.; Bacskay, G. B.; Haworth, N. L. Reactions of Phosphorus-Containing Species of Importance in the Catalytic Recombination of H + OH: Quantum Chemical and Kinetic Studies. *J. Phys. Chem. A* **2002**, *106* (45), 10825−10830.
(19) Weil, E. D.; Levchik, S. V. Flame Retardants, Phosphorus. In *Kirk-Othmer Encyclopedia of Chemical Technology*; John Wiley & Sons, Inc, 2017.
(20) Van Vranken, D. L. *Phosphorus Chemistry California*2016.
(21) Plane, J. M. C.; Feng, W.; Douglas, K. M. Phosphorus Chemistry in the Earth's Upper Atmosphere. *J. Geophys. Res.: Space Phys.* **2021**, *126* (10), No. e2021JA029881, DOI: 10.1029/2021JA029881.
(22) Kim, Y.; Kim, H.; Park, K. Theoretical Studies for Strong Hydrogen Bonds in Trimethyl Phosphate-(HNO3)n Complexes, n = 1−3. *Bull. Korean Chem. Soc.* **2002**, *23* (12), 1811−1815.
(23) George, L.; Viswanathan, K. S.; Singh, S. Ab Initio Study of Trimethyl Phosphate: Conformational Analysis, Dipole Moments, Vibrational Frequencies, and Barriers for Conformer Interconversion. *J. Phys. Chem. A* **1997**, *101* (13), 2459−2464.
(24) Reva, I.; Simão, A.; Fausto, R. Conformational Properties of Trimethyl Phosphate Monomer. *Chem. Phys. Lett.* **2005**, *406* (1−3), 126−136.
(25) Salmeia, K. A.; Fage, J.; Liang, S.; Gaan, S. An Overview of Mode of Action and Analytical Methods for Evaluation of Gas Phase Activities of Flame Retardants. *Polymers* **2015**, *7* (3), 504−526.
(26) Mendis, G. P.; Weiss, S. G.; Korey, M.; Boardman, C. R.; Dietenberger, M.; Youngblood, J. P.; Howarter, J. A. Phosphorylated Lignin as a Halogen-Free Flame Retardant Additive for Epoxy Composites. *Green Mater.* **2016**, *4* (4), 150−159, DOI: 10.1680/jgrma.16.00008.
(27) Knyazkov, D. A.; Bolshova, T. A.; Shvartsberg, V. M.; Chernov, A. A.; Korobeinichev, O. P. Inhibition of Premixed Flames of Methyl Methacrylate by Trimethylphosphate. *Proc. Combust. Inst.* **2021**, *38* (3), 4625−4633.
(28) Shvartsberg, V. M.; Shmakov, A. G.; Bolshova, T. A.; Korobeinichev, O. P. Mechanism for Inhibition of Atmospheric-Pressure Syngas/Air Flames by Trimethylphosphate. *Energy Fuels* **2012**, *26* (9), 5528−5536.
(29) Knyazkov, D. A.; Shvartsberg, V.; Gerasimov, I. E. Inhibition Of Combustion Of Dimethyl Ether/Air Mixture By Trimethylphosphate Additives. *Adv. Nonequilib. Processes* **2018**, 160−169.
(30) Korobeinichev, O. P.; Rybitskaya, I. V.; Shmakov, A. G.; Chernov, A. A.; Bolshova, T. A.; Shvartsberg, V. M. Mechanism of Inhibition of Hydrogen/Oxygen Flames of Various Compositions by Trimethyl Phosphate. *Kinet. Catal.* **2010**, *51* (2), 154−161.
(31) Matsumoto, K.; Martinez, M.; Gutel, T.; Mailley, S.; De Vito, E.; Patoux, S.; Inoue, K.; Utsugi, K. Stability of Trimethyl Phosphate Non-Flammable Based Electrolyte on the High Voltage Cathode (LiNi0.5Mn1.5O4). *J. Power Sources* **2015**, *273*, 1084−1088.
(32) Shiroudi, A.; Abdel-Rahman, M. A.; El-Nahas, A. M.; Altarawneh, M. Atmospheric Chemistry of Oxazole: The Mechanism and Kinetic Studies of the Oxidation Reaction Initiated by OH Radicals. *New J. Chem.* **2021**, *45* (4), 2237−2248.
(33) Korobeinichev, O. P.; Bolshova, T. A.; Shmakov, A. G.; Shvartsberg, V. M.; Rybitskaya, I. V.*Experimental Study And Modeling Of Inhibition Effect Of Dimethyl Methylphosphonate On Burning Velocity Of Stoichiometric Propane/Air Mixtures At Atmospheric Pressure, Proceedings of The Fourth Asia-Pacific Conference on Combustion*, 2005.
(34) Wu, J.; Bruce, F. N. O.; Bai, X.; Ren, X.; Li, Y. Insights into the Reaction Kinetics of Hydrazine-Based Fuels: A Comprehensive Review of Theoretical and Experimental Methods. *Energies* **2023**, *16* (16), No. 6006, DOI: 10.3390/en16166006.
(35) Mendes, J.; Zhou, C. W.; Curran, H. J. Theoretical Study of the Rate Constants for the Hydrogen Atom Abstraction Reactions of Esters with ȯH Radicals. *J. Phys. Chem. A* **2014**, *118* (27), 4889−4899.
(36) Korobeinichev, O. P.; Shmakov, A. G.; Shvartsberg, V. M. Chemical Transformations in Inhibited Flames over Range of Stoichiometry. In *Stoichiometry and Materials Science - When Numbers Matter*; InTech, 2012.
(37) Rong, C.; Zhao, D.; He, X.; Liu, S. Development and Applications of the Density-Based Theory of Chemical Reactivity. *J. Phys. Chem. Lett.* **2022**, *13* (48), 11191−11200.
(38) Korobeinichev, O. P.; Shvartsberg, V. M.; Shmakov, A. G.; Bolshova, T. A.; Jayaweera, T. M.; Melius, C. F.; Pitz, W. J.; Westbrook, C. K.; Curran, H. Flame Inhibition by Phosphorus-Containing Compounds in Lean and Rich Propane Flames. *Proc. Combust. Inst.* **2005**, *30* (2), 2353−2360.
(39) Jayaweera, T. M.; Melius, C. F.; Pitz, W. J.; Westbrook, C. K.; Korobeinichev, O. P.; Shvartsberg, V. M.; Shmakov, A. G.; Rybitskaya, I. V.; Curran, H. J. Flame Inhibition by Phosphorus-Containing Compounds over a Range of Equivalence Ratios. *Combust. Flame* **2005**, *140* (1−2), 103−115.
(40) Korobeinichev, O. P.; Ilyin, S. B.; Shvartsberg, V. M.; Chernov, A. A. The destruction chemistry of organophosphorus compounds in flames—I: quantitative determination of final phosphorus-containing species in hydrogen-oxygen flames. *Combust. Flame* **1999**, *118* (4), 718−726, DOI: 10.1016/S0010-2180(99)00030-9.
(41) Shmakov, A. G.; Korobeinichev, O. P.; Mebel, A. M.; Porfiriev, D. P.; Ghildina, A. R.; Osipova, K. N.; Knyazkov, D. A.; Gerasimov, I. E.; Liu, Z.; Yang, B. High-Temperature Thermal Decomposition of Triphenyl Phosphate Vapor in an Inert Medium: Flow Reactor Pyrolysis, Quantum Chemical Calculations, and Kinetic Modeling. *Combust. Flame* **2023**, *249*, No. 112614, DOI: 10.1016/j.combustflame.2022.112614.
(42) Zhu, Y.; Zhou, C. W. Chemical Kinetics Study of 1,3-Butadiene + HȮ2; Implications for Combustion Modeling and Simulation. *Combust. Flame* **2020**, *221*, 241−255.
(43) Neupane, S.; Rahman, R. K.; Baker, J.; Arafin, F.; Ninnemann, E.; Thurmond, K.; Wang, C. H.; Masunov, A. E.; Vasu, S. S. DMMP Pyrolysis and Oxidation Studies at High Temperature inside a Shock Tube Using Laser Absorption Measurements of CO. *Combust. Flame* **2020**, *214*, 14−24.

https://doi.org/10.1021/acsomega.3c07137
ACS Omega 2023, 8, 47134−47145

(44) National Center for Biotechnology Information. PubChem Compound Summary for CID 10541. https://pubchem.ncbi.nlm.nih.gov/compound/Trimethyl-phosphate (accessed August 30, 2023).
(45) Grimme, S.; Antony, J.; Ehrlich, S.; Krieg, H. A Consistent and Accurate Ab Initio Parametrization of Density Functional Dispersion Correction (DFT-D) for the 94 Elements H-Pu. *J. Chem. Phys.* **2010**, *132* (15), No. 154104, DOI: 10.1063/1.3382344.
(46) Liu, S.; Zhang, X. Chemical Concepts from Density Functional Theory. *Acta Phys. - Chim. Sin.* **2018**, *34* (6), 563−566.
(47) Marrazzini, G.; Giovannini, T.; Scavino, M.; Egidi, F.; Cappelli, C.; Koch, H. Multilevel Density Functional Theory. *J. Chem. Theory Comput.* **2021**, *17* (2), 791−803.
(48) Zhao, Y.; Truhlar, D. G. The M06 Suite of Density Functionals for Main Group Thermochemistry, Thermochemical Kinetics, Noncovalent Interactions, Excited States, and Transition Elements: Two New Functionals and Systematic Testing of Four M06-Class Functionals and 12 Other Functionals. *Theor. Chem. Acc.* **2008**, *120* (1−3), 215−241.
(49) Montgomery, J. A.; Frisch, M. J.; Ochterski, J. W.; Petersson, G. A. A Complete Basis Set Model Chemistry. VI. Use of Density Functional Geometries and Frequencies. *J. Chem. Phys.* **1999**, *110* (2−12), 2822−2827.
(50) Barker, J. R.; Nguyen, T. L.; Stanton, J. F.; Aieta, C.; Ceotto, M.; Gabas, F.; Kumar, T. J. D.; Li, C. G. L.; Lohr, L. L.; Maranzana, A.; Ortiz, N. F.; Preses, J. M.; Simmie, J. M.; Sonk, J. A.; Stimac, P. J. MultiWell-2014.1 Software Suite, 2014. https://multiwell.engin.umich.edu (accessed August 30, 2023).
(51) Masoumpour, M. S.; Daryanavard, M. The Kinetics and Dynamics of the Multichannel Multiwell Reaction of CO($1\sum^{+}$) with OH(2Π): Theoretical Investigation. *SN Appl. Sci.* **2020**, *2* (3), No. 481, DOI: 10.1007/s42452-020-2299-x.
(52) Goldsmith, C. F.; Magoon, G. R.; Green, W. H. Database of Small Molecule Thermochemistry for Combustion. *J. Phys. Chem. A* **2012**, *116* (36), 9033−9047.
(53) Sun, Y.; Zhou, C. W.; Somers, K. P.; Curran, H. J. Ab Initio/Transition-State Theory Study of the Reactions of $\dot{C}$5H9 Species of Relevance to 1,3-Pentadiene, Part I: Potential Energy Surfaces, Thermochemistry, and High-Pressure Limiting Rate Constants. *J. Phys. Chem. A* **2019**, *123* (42), 9019−9052.
(54) Sun, Y.; Zhou, C. W.; Somers, K. P.; Curran, H. J. An Ab Initio/Transition State Theory Study of the Reactions of $\dot{C}$5H9Species of Relevance to 1,3-Pentadiene, Part II: Pressure Dependent Rate Constants and Implications for Combustion Modeling. *J. Phys. Chem. A* **2020**, *124* (23), 4605−4631.
(55) Cioslowski, J.; Grzebielucha, E. Zero-Point Vibrational Energies of Spherical Coulomb Crystals. *J. Chem. Phys.* **2009**, *130* (9), No. 094902, DOI: 10.1063/1.3077028.
(56) Kesharwani, M. K.; Brauer, B.; Martin, J. M. L. Frequency and Zero-Point Vibrational Energy Scale Factors for Double-Hybrid Density Functionals (and Other Selected Methods): Can Anharmonic Force Fields Be Avoided? *J. Phys. Chem. A* **2015**, *119* (9), 1701−1714.
(57) Grev, R. S.; Janssen, C. L.; Schaefer, H. F. Concerning Zero-Point Vibrational Energy Corrections to Electronic Energies. *J. Chem. Phys.* **1991**, *95* (7), 5128−5132.
(58) Curtiss, L. A.; Redfern, P. C.; Raghavachari, K. Assessment of Gaussian-3 and Density-Functional Theories on the G3/05 Test Set of Experimental Energies. *J. Chem. Phys.* **2005**, *123* (12), No. 124107, DOI: 10.1063/1.2039080.
(59) Curtiss, L. A.; Redfern, P. C.; Raghavachari, K. Gaussian-4 Theory. *J. Chem. Phys.* **2007**, *126* (8), No. 084108, DOI: 10.1063/1.2436888.
(60) Curtiss, L. A.; Raghavachari, K.; Redfern, P. C.; Rassolov, V.; Pople, J. A. Gaussian-3 (G3) Theory for Molecules Containing First and Second-Row Atoms. *J. Chem. Phys.* **1998**, *109* (18), 7764−7776.
(61) Curtiss, L. A.; Raghavachari, K.; Redfern, P. C.; Pople, J. A. Assessment of Gaussian-2 and Density Functional Theories for the Computation of Enthalpies of Formation. *J. Chem. Phys.* **1997**, *106* (3), 1063−1079.
(62) Georgievskii, Y.; Miller, J. A.; Burke, M. P.; Klippenstein, S. J. Reformulation and Solution of the Master Equation for Multiple-Well Chemical Reactions. *J. Phys. Chem. A* **2013**, *117* (46), 12146−12154.
(63) Mai, T. V. T.; Bui, T. Q.; Nhung, N. T. A.; Quy, P. T.; Shrestha, K. P.; Mauss, F.; Giri, B. R.; Huynh, L. K. An Ab Initio RRKM-Based Master Equation Study for Kinetics of OH-Initiated Oxidation of 2-Methyltetrahydrofuran and Its Implications in Kinetic Modeling. *Energies* **2023**, *16* (9), No. 3730, DOI: 10.3390/en16093730.
(64) Shao, Y.; Molnar, L. F.; Jung, Y.; Kussmann, J.; Ochsenfeld, C.; Brown, S. T.; Gilbert, A. T. B.; Slipchenko, L. V.; Levchenko, S. V.; O'Neill, D. P.; DiStasio, R. A.; Lochan, R. C.; Wang, T.; Beran, G. J. O.; Besley, N. A.; Herbert, J. M.; Yeh Lin, C.; Van Voorhis, T.; Chien, S. H.; Sodt, A.; Steele, R. P.; Rassolov, V. A.; Maslen, P. E.; Korambath, P. P.; Adamson, R. D.; Austin, B.; Baker, J.; Byrd, E. F. C.; Dachsel, H.; Doerksen, R. J.; Dreuw, A.; Dunietz, B. D.; Dutoi, A. D.; Furlani, T. R.; Gwaltney, S. R.; Heyden, A.; Hirata, S.; Hsu, C. P.; Kedziora, G.; Khalliulin, R. Z.; Klunzinger, P.; Lee, A. M.; Lee, M. S.; Liang, W.; Lotan, I.; Nair, N.; Peters, B.; Proynov, E. I.; Pieniazek, P. A.; Rhee, Y. M.; Ritchie, J.; Rosta, E.; Sherrill, C. D.; Simmonett, A. C.; Subotnik, J. E.; Woodcock, H. L.; Zhang, W.; Bell, A. T.; Chakraborty, A. K.; Chipman, D. M.; Keil, F. J.; Warshel, A.; Hehre, W. J.; Schaefer, H. F.; Kong, J.; Krylov, A. I.; Gill, P. M. W.; Head-Gordon, M. Advances in Methods and Algorithms in a Modern Quantum Chemistry Program Package. *Phys. Chem. Chem. Phys.* **2006**, *8* (27), 3172−3191, DOI: 10.1039/B517914A.
(65) Manby, F.; Alexander, B.; Callum, B.; Sebastian, L.; Rocco, M.; Kaito, M.; Casper, S.; Takashi, T.; Matthew, W.; Timothy, W.; Zack, W.et al.Entos: A Quantum Molecular Simulation Package *ChemRxiv. Cambridge: Cambridge Open Engage* 2019.
(66) Ramanathan, N.; Sundararajan, K. Influence of Inert Matrixes on the Conformational Switching of Trimethyl Phosphate at Low Temperatures through Thermal Effects. *J. Mol. Spectrosc.* **2018**, *349*, 23−31.
(67) St John, P.; Guan, Y.; Kim, Y.; Kim, S. BDE-Db: A Collection of 290,664 Homolytic Bond Dissociation Enthalpies for Small Organic Molecules. *Figshare* 2019.
(68) Owens, F. J. Structure and Stability of Solvation Complexes of Trimethyl Phosphate and Dimethyl Methyl Phosphonate. *Int. J. Quantum Chem.* **2017**, *117* (7), No. e25347, DOI: 10.1002/qua.25347.
(69) Neupane, S.; Rahman, R. K.; Masunov, A. E.; Vasu, S. S. Theoretical Calculation of Reaction Rates and Combustion Kinetic Modeling Study of Triethyl Phosphate (TEP). *J. Phys. Chem. A* **2019**, *123* (22), 4764−4775.
(70) Koshlyakov, P. V.; Barkova, D. A.; Gerasimov, I. E.; Chesnokov, E. N.; Zhang, X.; Krasnoperov, L. N. Kinetics of the Gas-Phase Reaction of Hydroxyl Radicals with Trimethyl Phosphate over the 273−837 K Temperature Range. *RSC Adv.* **2021**, *11* (23), 14121−14131.
(71) Tuazon, C.; Atkinson, R.; Aschmann, S. M.; Arey, J.; Winer, A. M.; Pitts, J. N. The Chemistry of Aquatic Pollutants. *Tech. Bull.* **1986**, *2* (0), 2807−2815.
(72) Aschmann, S. M.; Long, W. D.; Atkinson, R. Rate Constants for the Gas-Phase Reactions of OH Radicals with Dimethyl Phosphonate over the Temperature Range of 278−351 K and for a Series of Other Organophosphorus Compounds at ∼ 280 K. *J. Phys. Chem. A* **2008**, *112* (21), 4793−4799.
(73) Burns, D. S.; Cory, M. G.; Taylor, D. E.; Bunte, S. W.; Runge, K.; Vasey, J. L. A Comparison of Primary and Secondary Hydrogen Abstraction from Organophosphates by Hydroxyl Radical. *Int. J. Chem. Kinet.* **2013**, *45* (3), 187−201.

https://doi.org/10.1021/acsomega.3c07137
ACS Omega 2023, 8, 47134−47145